In-Gap Spin Excitations and Finite Triplet Lifetimes in the Dilute Singlet Ground State System $SrCu_{2-x}Mg_x(BO_3)_2$

S. Haravifard,[1] S. R. Dunsiger,[1] S. El Shawish,[2] B. D. Gaulin,[1,3] H. A. Dabkowska,[1] M. T. F. Telling,[4] T. G. Perring,[4] and J. Bonča[2,5]

[1]*Department of Physics and Astronomy, McMaster University, Hamilton, Ontario L8S 4M1, Canada*
[2]*J. Stefan Institute, SI-1000 Ljubljana, Slovenia*
[3]*Canadian Institute for Advanced Research, 180 Dundas Street W, Toronto, Ontario M5G 1Z8, Canada*
[4]*Rutherford Appleton Laboratory, ISIS Pulsed Neutron Facility, Chilton, Didcot, Oxon OX110QX, United Kingdom*
[5]*Faculty of Mathematics and Physics, University of Ljubljana, SI-1000 Ljubljana, Slovenia*

(Received 11 August 2006; published 14 December 2006)

High resolution neutron scattering measurements on a single crystal of $SrCu_{2-x}Mg_x(BO_3)_2$ with $x \sim 0.05$ reveal the presence of new spin excitations within the gap of this quasi-two-dimensional, singlet ground state system. The application of a magnetic field induces Zeeman-split states associated with $S = 1/2$ unpaired spins which are antiferromagnetically correlated with the bulk singlet. Substantial broadening of both the one- and two-triplet excitations in the doped single crystal is observed, as compared with pure $SrCu_2(BO_3)_2$. Theoretical calculations using a variational algorithm and a single quenched magnetic vacancy on an infinite lattice are shown to qualitatively account for these effects.

DOI: 10.1103/PhysRevLett.97.247206 PACS numbers: 75.25.+z, 61.12.Ex, 75.40.Gb

Quasi-two-dimensional quantum magnets which display collective singlet or spin gap behavior are very topical due to the novelty of their ground states [1] and their relation to high temperature superconductivity in the copper oxides. There are relatively few such materials, and crystal growth difficulties have further limited their study in single crystal form. $SrCu_2(BO_3)_2$ is established as a realization of the two-dimensional Shastry-Sutherland model [2] for interacting $S = 1/2$ dimers [3,4]. It is comprised of well separated layers of Cu^{2+}, $S = 1/2$ orthogonal dimers arranged on a square lattice. The material crystallizes into the tetragonal space group $I\bar{4}2m$ with room temperature lattice parameters of $a = 8.995$ Å, $c = 6.649$ Å [5].

$SrCu_2(BO_3)_2$ has been well studied by an array of experimental techniques, which show it to possess a nonmagnetic ground state. In particular, earlier neutron [6–9] and ESR spectroscopies [10,11] have established the leading terms in its microscopic Hamiltonian:

$$\mathcal{H} = J\sum_{nn} \mathbf{S_i} \cdot \mathbf{S_j} + J'\sum_{nnn} \mathbf{S_i} \cdot \mathbf{S_j} + g\mu_B \mathbf{H} \cdot \sum_i \mathbf{S_i}, \quad (1)$$

where J is the exchange interaction within the dimers and J' is the exchange interaction between $S = 1/2$ spins on neighboring dimers. Subleading Dzyaloshinskii-Moriya interactions weakly split the three triplet modes even in zero applied magnetic field [7–9,12].

Both the exchange interactions are antiferromagnetic and their ratio $x = \frac{J'}{J}$ has been estimated between 0.68 and 0.60, with more recent refinements being smaller. Such a quantum magnet is known to possess a singlet ground state so long as x is sufficiently small [13]. All of these estimates place $SrCu_2(BO_3)_2$ on the low side of the critical value of x at which a quantum phase transition occurs between a four sublattice Néel state and a collective singlet state.

In a finite magnetic field, much interest has focused on a finite magnetization which develops at fields beyond ~20 T, wherein the lowest energy of the three triplet states has been driven to zero energy [4,14–16]. The magnetic field acts as a chemical potential for the triplet density within the quasi-two-dimensional planes. Magnetization plateaus ensue at higher fields, corresponding to Bose condensation of the triplets at certain densities.

While pure $SrCu_2(BO_3)_2$ has been well studied, there is little information on this quantum magnet in the presence of dopants, and no reports on doped single crystals. This problem is very interesting by analogy with the remarkable properties of doped quasi-two-dimensional Mott insulators and high temperature superconductivity [17]. $SrCu_2(BO_3)_2$ is itself a Mott insulator, and the theory of doped Mott insulators on the Shastry-Sutherland lattice shows the possibility of several different superconducting phases as a function of doping [18–20]. Several doping studies of $SrCu_2(BO_3)_2$ have been reported on polycrystalline samples wherein Al, La, Na, and Y substitute at the Sr site and Mg substitutes at the Cu site [21].

In this Letter we report high resolution time-of-flight neutron scattering measurements on large single crystals of $SrCu_{2-x}Mg_x(^{11}BO_3)_2$ and $SrCu_2(^{11}BO_3)_2$. These measurements show that doping of the magnetic Cu^{2+} site with nonmagnetic, isoelectronic Mg^{2+} at the 2.5% level introduces new magnetic excitations into the singlet energy gap, and gives a finite lifetime to all three single-triplet excitations, while also substantially broadening the two-triplet bound state.

Two single crystal samples, $SrCu_2(^{11}BO_3)_2$ and $SrCu_{2-x}Mg_x(^{11}BO_3)_2$, were grown by floating zone image

furnace techniques at a rate of 0.2 mm/h in an O_2 atmosphere. The crystals were of almost identical cylindrical shape, with approximate dimensions of 4.5 cm in length by 0.6 cm in diameter. These samples were grown using ^{11}B to avoid the high neutron absorption cross section of natural boron. Time-of-flight neutron scattering measurements were performed using the OSIRIS spectrometer [22] at the ISIS Pulsed Neutron Source of the Rutherford Appleton Laboratory. OSIRIS is an indirect geometry time-of-flight spectrometer which employs an array of pyrolytic graphite monochromators to energy analyze the scattered neutron beam. The data were collected using the 004 analyzing reflection afforded by pyrolytic graphite, such that the scattered energy was 7.375 meV. The $[H, 0, L]$ plane of both crystals was coincident with the horizontal scattering plane, and the samples were mounted in a 7 T vertical, $[0, K, 0]$, field magnet cryostat.

Figure 1 shows representative time-of-flight neutron scattering data, taken at $T = 2$ K and $H = 0$ and 7 T for $SrCu_2(BO_3)_2$ [panels (a) and (c)] and for $SrCu_{2-x}Mg_x(BO_3)_2$ [panels (b) and (d)]. These data were integrated along L, in which direction the spin excitations show little dispersion [9]. Note the logarithmic energy and intensity scales. The splitting of the triplet excitations near 3 meV on application of the 7 T magnetic field is clear. In finite field, weak dispersion of the triplet excitations as a function of wave vector H is seen, and this has been attributed to subleading terms in the spin Hamiltonian. There are several qualitative features evident on examination of these data. The one-triplet excitations show significantly greater breadth in energy in $SrCu_{2-x}Mg_x(BO_3)_2$ than in $SrCu_2(BO_3)_2$. In addition, application of a $H = 7$ T magnetic field gives rise to an inelastic peak at $g\mu_B H = 0.8$ meV in $H = 7$ T, which is centered at $[H \sim 1.4, 0, 0]$ in $\mathbf{Q}$ space, but extends in wave vector H to almost $[H \sim 3, 0, 0]$.

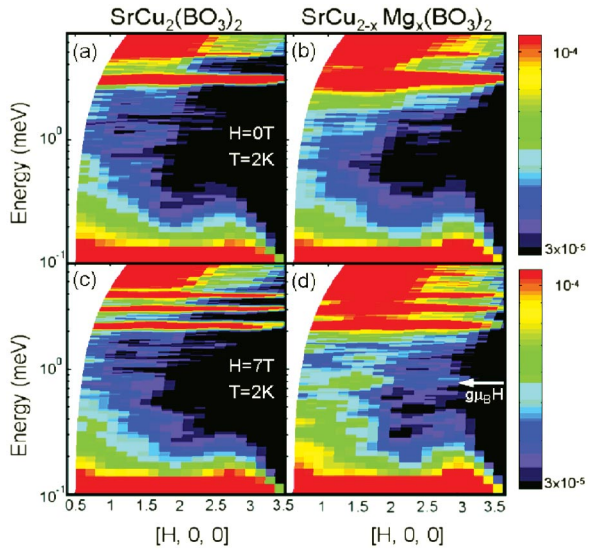

FIG. 1 (color). Panels (a) and (c) show neutron scattering data from $SrCu_2(BO_3)_2$ at $T = 2$ K. The scattering has been integrated along L, and we show data in a magnetic field of zero and 7 T. Panels (b) and (d) show the same data for $SrCu_{2-x}Mg_x(BO_3)_2$. The Zeeman-split $S = 1/2$ level in $SrCu_{2-x}Mg_x(BO_3)_2$ in $H = 7$ T at $g\mu_B H = 0.8$ meV is indicated in panel (d).

Figures 2(b) and 2(d) show the same experimental data as in Fig. 1, now integrated in a wave vector along L and also in H between $H = 1$ r.l.u. and $H = 3$ r.l.u. (where r.l.u. is reciprocal lattice units) and plotted as a function of energy. The data in a magnetic field of 0 and 7 T are shown in Figs. 2(b) and 2(d), respectively. The extra breadth in both the single-triplet excitations and the two-triplet bound states above it is clear. Broad inelastic peaks appear within the gap, which possess little magnetic field dependence, indicating a longitudinal nature. Sharp, field-induced inelastic scattering at $\hbar\omega \sim 0.8$ meV is also evident.

Numerical calculations have also been carried out using a new variational approach [23] to solve the model of a single quenched impurity on the two-dimensional Shastry-Sutherland lattice. This method generates a variational space by successively applying the off-diagonal parts of the Hamiltonian [Eq. (1)] on the starting approximation for the single impurity ground state, which consists of a free spin 1/2 neighboring the impurity site, embedded within a dimerized background. The resulting small spin polaron structure (the unpaired spin surrounded by triplet fluctuations) and exponential growth of the variational space with each iteration guarantee good convergence of the spin

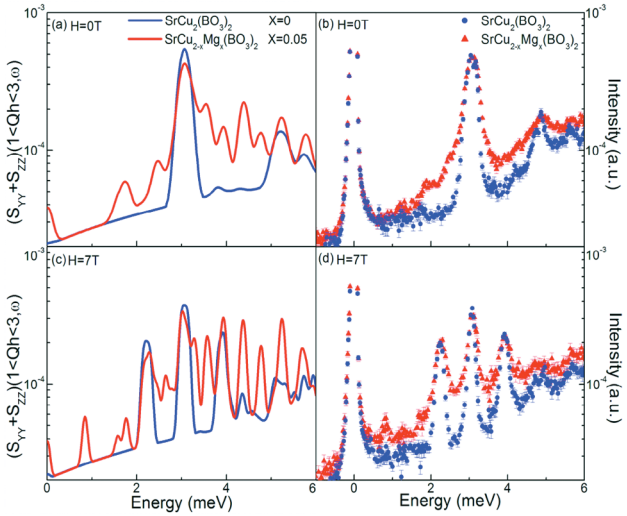

FIG. 2 (color). Panels (b) and (d) show inelastic neutron scattering data for both $SrCu_2(BO_3)_2$ and $SrCu_{2-x}Mg_x(BO_3)_2$ in $H = 0$ (b) and $H = 7$ T (d). These data have been integrated in $\mathbf{Q}$ between $H = 1$ and $H = 3$ and over all L. Clearly the one- and two-triplet excitations are considerably broader in energy in $SrCu_{2-x}Mg_x(BO_3)_2$ as compared with $SrCu_2(BO_3)_2$, and in-gap states are introduced on doping. Panels (a) and (c) show the numerical calculation for $S^{zz}(\mathbf{Q}, \omega) + S^{yy}(\mathbf{Q}, \omega)$, using $J = 76.8$ K and $J'/J = 0.62$.

polaron ground state, as well as for the lowest energy excited states [23]. For energies below ~3 meV the method provides accurate and converged results for both the longitudinal, $S^{zz}(\mathbf{Q}, \omega)$, as well as the transverse, $S^{yy}(\mathbf{Q}, \omega)$, components of the dynamical spin structure factor. These are compared directly to the neutron scattering experiments in Fig. 2.

Figures 2(a) and 2(c) show the calculated $S^{zz}(\mathbf{Q}, \omega) + S^{yy}(\mathbf{Q}, \omega)$, integrated over the same range of wave vectors as the experimental data, and at magnetic fields of 0 (a) and 7 T (c). The comparison between theory and experiment is qualitatively good. The numerical results confirm that quenched magnetic vacancies induce in-gap states, a substantial spectral weight below the zero field gap energy of ~3 meV. A component of these in-gap states shows little magnetic field dependence and appears in the $S^{zz}(\mathbf{Q}, \omega)$ longitudinal channel. The calculation also shows the $g\mu_B H$ transverse, $S^{yy}(\mathbf{Q}, \omega)$, excitation in finite magnetic field. Furthermore, the calculation [23] allows a determination of the spatial distribution of the spin polaron $S = 1/2$ degree of freedom and its low lying excited states, and these allow a quantitative comparison to the experiment.

Figure 3 shows the $\mathbf{Q}$ dependence of the scattering around $g\mu_B H = 0.8$ meV in an applied magnetic field of 7 T in both $SrCu_2(BO_3)_2$ (a) and $SrCu_{2-x}Mg_x(BO_3)_2$ (b). This scattering is integrated in wave vector over L and in energy between 0.6 meV $< \hbar\omega <$ 1 meV, and is shown in a magnetic field of both 0 and 7 T. Figure 3(a) shows the absence of a magnetic field-induced signal in $SrCu_2(BO_3)_2$ within this energy range. Figure 3(b) shows a clear field-induced signal in $SrCu_{2-x}Mg_x(BO_3)_2$, which peaks at $[H \sim 1.4, 0, 0]$ but extends out to almost $[H \sim 3.0, 0, 0]$.

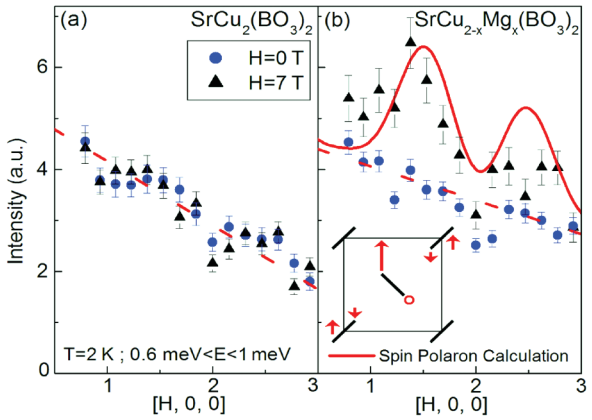

FIG. 3 (color). $\mathbf{Q}$ scans are shown at $T = 2$ K for both $SrCu_2(BO_3)_2$ (a) and $SrCu_{2-x}Mg_x(BO_3)_2$ (b), which integrate in energy between 0.6 and 1 meV. This energy range captures the Zeeman energy $g\mu_B H = 0.8$ meV appropriate to $g = 2$ and $H = 7$ T. (b) shows a comparison between the experimental $\mathbf{Q}$ dependence of this scattering with the calculated form described in the text. The inset of (b) shows a schematic diagram of the local structure of a single spin polaron, where the open circle indicates the impurity.

This field-induced scattering is attributed to Zeeman-split $S = 1/2$ states associated with the $S = 1/2$ moment in a dimer whose partner site is occupied by a quenched, nonmagnetic Mg^{2+} ion. This field-induced inelastic scattering is very similar to that associated with end states in Haldane spin chains, such as those that occur in $Y_2BaNi_{1-x}Mg_xO_5$ [24]. In this case, quenched, nonmagnetic Mg^{2+} ions produce finite $S = 1$ magnetic chains. Spin 1/2 degrees of freedom arise at the end of finite chains of $S = 1$ magnetic moments, as one of the two effective $S = 1/2$ degrees of freedom making up the $S = 1$ moments lacks a partner with which to form a singlet. Such excitations occur at an energy of $g\mu_B H$ in finite field and display a wave-vector dependence which indicates antiferromagnetic correlations into the collective singlet of the chain segment. More dramatically, nonmagnetic impurities induce antiferromagnetic long range order in the doped quasi-one-dimensional $S = 1/2$ system $CuGeO_3$, which coexists with a singlet, spin-Peierls ground state [25].

The wave-vector dependence of the magnetic field-induced spin excitation at 0.8 meV can be attributed to the structure of the spin polaron [23], whose ground state possesses strong antiferromagnetic correlations with neighboring dimers, transverse to the dimer containing the impurity site. This local spin structure is shown schematically in the inset of Fig. 3(b). The structure factor for the Zeeman transition within the $S^z = \pm 1/2$ polaron doublet can be calculated to first nontrivial order in $J'/J = 0.62$, and this is scaled by the Cu^{2+} magnetic form factor and compared to our measurement in Fig. 3(b). Within this calculation [23], the spin polaron is formed by five variational states, the largest of which corresponds to the unpaired spin surrounded by spin singlets on all other dimers. The other four variational states have additional spin triplets located transverse to the dimer containing the impurity, consistent with the schematic diagram in the inset of Fig. 3(b). While the agreement between the calculation and experiment is not perfect, the calculation captures the general $\mathbf{Q}$ dependence of the excitation.

Figure 4(a) shows representative data with accompanying fits used to extract the lifetimes of the one-triplet excitations as a function of doping and temperature in a magnetic field of 7 T. These data are integrated in $\mathbf{Q}$ along L and over a narrow range in wave vector H around $H = 1.5$, and these cuts approximate constant-$\mathbf{Q}$ scans. Similar analysis was performed around wave vector $H = 2.0$ and 2.5 to look for variation in the one-triplet lifetimes as a function of $\mathbf{Q}$ along $[H, 0, 0]$. The data were fit to the sum of three identical damped harmonic oscillators (DHOs):

$$S(\mathbf{Q}, \omega, T) = \chi(\mathbf{Q}, T)\frac{1}{1 - \exp(-\frac{\omega}{kT})} \times \left[\frac{4\omega\Gamma_{\mathbf{Q},T}/\pi}{(\omega^2 - \Omega_{\mathbf{Q},T}^2)^2 + 4\omega^2\Gamma_{\mathbf{Q},T}^2}\right], \quad (2)$$

where $\chi(\mathbf{Q}, T)$ is the momentum-dependent susceptibility.

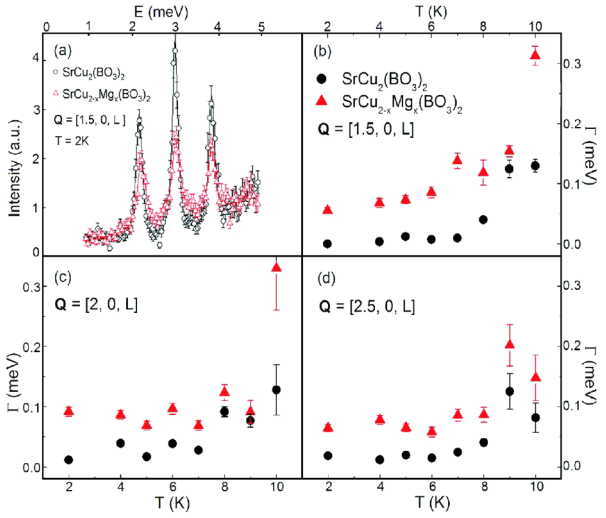

FIG. 4 (color online). (a) Cuts of the data simulating constant-**Q** scans at $(1.5, 0, L)$, integrated along L, are shown for $SrCu_2(BO_3)_2$ and $SrCu_{2-x}Mg_x(BO_3)_2$. Resolution convoluted fits to the data are shown as the solid lines, and the description of the data is excellent. Such fits allow us to extract the triplet excitation lifetimes $(1/\Gamma)$, which are shown in (b), (c), and (d) for wave vectors $(1.5, 0, L)$, $(2, 0, L)$, and $(2.5, 0, L)$, respectively, as a function of temperature.

The renormalized DHO frequency, $\Omega_{\mathbf{Q}}$, has contributions from the oscillation frequency, $\omega_{\mathbf{Q},T}$, and the damping coefficient, $\Gamma_{\mathbf{Q},T}$, and is given by $\Omega^2_{\mathbf{Q},T} = \omega^2_{\mathbf{Q},T} + \Gamma^2_{\mathbf{Q},T}$.

Equation (2) was convoluted with an appropriate resolution function and fit to the data. The results are shown in Figs. 4(b)–4(d), for wave vectors $H = 1.5$, 2.0, and 2.5, respectively. The extracted lifetimes show little or no systematic variation with wave vector H, but a finite one-triplet lifetime is observed in $SrCu_{2-x}Mg_x(BO_3)_2$ at all temperatures, in contrast to $SrCu_2(BO_3)_2$, where the low temperature one-triplet lifetimes are very long compared with the resolution of the spectrometer. In both $SrCu_{2-x}Mg_x(BO_3)_2$ and $SrCu_2(BO_3)_2$, the thermal destruction of the collective singlet ground state near $\sim$10 K is characterized by a rapid decrease in the one-triplet lifetime $(1/\Gamma)$ on warming, with little or no softening of the one-triplet excitation energies.

As mentioned previously, the theoretical results for $S^{zz}(\mathbf{Q}, \omega) + S^{yy}(\mathbf{Q}, \omega)$ are not well converged for energies of $\sim$3 meV and greater. Nonetheless, the additional broad spectral weight, albeit in the form of inelastic peaks [26] which are not observed experimentally, around the calculated one- and two-triplet energies seen in Figs. 2(a) and 2(c) is consistent with finite triplet lifetimes in the presence of a single quenched magnetic vacancy. The fact that finite lifetimes of the triplet excitations are observed on doping with nonmagnetic vacancies at the low 2.5% level may well be a consequence of the extended, spin polaron nature of the induced hole in the singlet ground state of $SrCu_{2-x}Mg_x(BO_3)_2$.

We wish to acknowledge expert technical support from the ISIS User Group. This work was supported by NSERC of Canada, and the Slovenian Research Agency under Contract No. PI-0044.

[1] See, for example, E. Dagotto and T. M. Rice, Science **271**, 618 (1996); *Dynamical Properties of Unconventional Magnetic Systems*, edited by A. T. Skjeltorp and D. Sherrington, NATO ASI, Ser. E, Vol. 349 (Kluwer Academic Publishers, Boston, 1998).
[2] B. S. Shastry and B. Sutherland, Physica (Amsterdam) **108B+C**, 1069 (1981).
[3] S. Miyahara and K. Ueda, Phys. Rev. Lett. **82**, 3701 (1999).
[4] H. Kageyama *et al.*, Phys. Rev. Lett. **82**, 3168 (1999).
[5] R. W. Smith and D. A. Keszler, J. Solid State Chem. **93**, 430 (1991).
[6] H. Kageyama *et al.*, Phys. Rev. Lett. **84**, 5876 (2000).
[7] O. Cepas *et al.*, Phys. Rev. Lett. **87**, 167205 (2001).
[8] K. Kakurai, in *Quantum Properties of Low Dimensional Antiferromagnets*, edited by A. Ajiro and J. P. Boucher (Kyushu University Press, Fukuoka, 2002).
[9] B. D. Gaulin *et al.*, Phys. Rev. Lett. **93**, 267202 (2004).
[10] A. Zorko *et al.*, Phys. Rev. B **69**, 174420 (2004).
[11] H. Nojiri, H. Kageyama, Y. Ueda, and M. Motokawa, J. Phys. Soc. Jpn. **72**, 3243 (2003).
[12] S. El Shawish, J. Bonča, and I. Sega, Phys. Rev. B **72**, 184409 (2005).
[13] M. Miyahara and K. Ueda, J. Phys. Condens. Matter **15**, R327 (2003).
[14] K. Kodama *et al.*, Science **298**, 395 (2002).
[15] K. Onizuka *et al.*, J. Phys. Soc. Jpn. **69**, 1016 (2000).
[16] G. A. Jorge *et al.*, Phys. Rev. B **71**, 092403 (2005).
[17] See, for example, J. Orenstein and A. J. Millis, Science **288**, 468 (2000).
[18] B. S. Shastry and B. Kumar, Prog. Theor. Phys. Suppl. **145**, 1 (2002).
[19] T. Kimura, K. Kuroki, R. Arita, and H. Aoki, Phys. Rev. B **69**, 054501 (2004).
[20] C-H. Chung and Y. B. Kim, Phys. Rev. Lett. **93**, 207004 (2004).
[21] G. T. Liu, J. L. Luo, N. L. Wang, X. N. Jing, D. Jin, T. Xiang, and Z. H. Wu, Phys. Rev. B **71**, 014441 (2005).
[22] M. T. F. Telling and K. H. Andersen, Phys. Chem. Chem. Phys. **7**, 1255 (2005).
[23] S. El Shawish and J. Bonča, cond-mat/0607753 [Phys. Rev. B (to be published)].
[24] M. Kenzelmann *et al.*, Phys. Rev. Lett. **90**, 087202 (2003).
[25] S. B. Oseroff *et al.*, Phys. Rev. Lett. **74**, 1450 (1995); K. M. Kojima *et al.*, Phys. Rev. Lett. **79**, 503 (1997).
[26] Our analysis shows that with increasing Hilbert space these additional peaks become denser while they remain centered at one- and two-triplet peaks. In the thermodynamic limit these emerging peaks lead to broadening of triplet lines.